



Cross-phase-modulation-induced temporal reflection and waveguiding of optical pulses

BRENT W. PLANSINIS,^{1,2,*} WILLIAM R. DONALDSON,² AND GOVIND P. AGRAWAL^{1,2}

¹The Institute of Optics, University of Rochester, Rochester, New York 14627, USA

²Laboratory for Laser Energetics, University of Rochester, 250 E. River Road, Rochester, New York 14623, USA

*Corresponding author: bplansin@ur.rochester.edu

Received 23 October 2017; revised 24 December 2017; accepted 28 December 2017; posted 3 January 2018 (Doc. ID 309753); published 31 January 2018

Cross-phase modulation (XPM) is commonly viewed as a nonlinear process that chirps a probe pulse and modifies its spectrum when an intense pump pulse overlaps with it. Here we present an alternative view of XPM in which the pump pulse creates a moving refractive-index boundary that splits the probe pulse into two parts with distinct optical spectra through temporal reflection and refraction inside a dispersive nonlinear medium. The probe even undergoes a temporal version of total internal reflection for sufficiently intense pump pulses, a phenomenon that can be exploited for making temporal waveguides. We investigate the practical conditions under which XPM can be exploited for temporal reflection and waveguiding. The width and shape of the pump pulses as well as the nature of the medium dispersion at the pump and probe wavelengths (normal versus anomalous) play important roles. The super-Gaussian shape of a pump pulse is particularly helpful because of the relatively sharp edges of the super-Gaussian shape. When the pump wavelength lies in the anomalous-dispersion regime, the pump pulse can form a soliton, whose unique properties can be exploited to our advantage. We also discuss a potential application of XPM-induced temporal waveguides for compensating for timing jitter. © 2018 Optical Society of America

OCIS codes: (190.5530) Pulse propagation and temporal solitons; (320.7110) Ultrafast nonlinear optics.

<https://doi.org/10.1364/JOSAB.35.000436>

1. INTRODUCTION

Cross-phase modulation (XPM) is a nonlinear optical process that has been studied extensively and is discussed in detail in many optics texts [1–3]. In a typical pump-probe configuration, XPM allows the intense pump pulse to impart a time-dependent phase shift onto a much weaker probe pulse, leading to changes in the spectrum of the probe pulse. Recently, there has been growing interest in the role XPM plays during the collision of a weak dispersive wave with a soliton, leading to the so-called soliton scattering, where the dispersive wave changes frequency as it bounces off the soliton [4–9]. The same process is being studied as an optical analog of gravity and Hawking radiation [10–14] as well as for pulse trapping [15–20].

Temporal analogs of reflection and refraction, which occur when an optical pulse arrives at a temporal boundary across which the refractive index changes suddenly in time, have been the focus of several studies [21–26]. Earlier works on this topic focused on the case of a nondispersive medium whose refractive index changed across the entire medium at a single instant in time [21–23], or when a counterpropagating boundary shifted the refractive index of the medium [27,28]. Recently, we have found the temporal analogs of reflection and refraction inside a dispersive medium when an optical pulse crosses a moving

refractive-index boundary [26,29]. More specifically, as the optical pulse crosses the boundary, it splits into two parts with different spectra that behave like reflected and transmitted pulses. Unlike the reflection occurring at a static spatial boundary, the reflected pulse continues to propagate forward in space, but its group velocity changes (owing to a spectral shift) such that this part of the pulse appears to recede from the boundary. If the index change across the pulse is large enough, the pulse can even undergo a temporal analog of total internal reflection (TIR) at a temporal boundary. Two of such moving temporal boundaries can then be used to create a temporal waveguide to confine an optical pulse to a narrow temporal region [30,31].

One way to create a moving temporal boundary is to employ the nonlinear phenomenon of XPM using a pump-probe configuration. When a dispersive medium exhibits the Kerr nonlinearity, the refractive index is higher in the temporal region inside the pulse, and we can view the edge of the pump pulse as a moving refractive-index boundary. From this point of view, soliton scattering is simply the reflection of the probe (a dispersive wave) from the moving boundary created by either the leading or trailing edge of the pump (the soliton). This way of looking at XPM is quite distinct from the traditional view in

which the pump modulates the phase of the probe, resulting in frequency chirping. In this paper, we explore the use of XPM to create temporal boundaries and study how XPM can be employed to produce temporal reflection and to make temporal waveguides.

This paper is organized as follows: Section 2 discusses what properties the dispersive medium must have to observe XPM-induced reflection and refraction by examining the cases of a Gaussian-shaped pump pulse and a solitonic pump pulse. The same pulse shapes are used in Section 3 to discuss how XPM can be employed to make a temporal waveguide. Section 4 focuses on one potential application of such waveguides by showing that XPM can be used to remove interpulse jitter for two lasers with synchronized repetition rates. The main results are summarized in Section 5.

2. PUMP-PROBE CONFIGURATION

We consider pump and probe pulses launched at different wavelengths and propagating inside a dispersive nonlinear waveguide such as an optical fiber. Assuming that both pulses are polarized linearly along the same direction, their evolution is governed by the two well-known coupled nonlinear Schrödinger equations [3]:

$$\frac{\partial A_1}{\partial z} + \frac{i\beta_{21}}{2} \frac{\partial^2 A_1}{\partial t^2} - \frac{\alpha}{2} A_1 = i\gamma_1(|A_1|^2 + 2|A_2|^2)A_1, \quad (1)$$

$$\frac{\partial A_2}{\partial z} + \Delta\beta_1 \frac{\partial A_2}{\partial t} + \frac{i\beta_{22}}{2} \frac{\partial^2 A_2}{\partial t^2} = i\gamma_2(|A_2|^2 + 2|A_1|^2)A_2, \quad (2)$$

where $A_1(z, t)$ is the slowly varying envelope of the pump pulse and $A_2(z, t)$ is that of the probe pulse. The time $t = T - \beta_{11}z$ is measured in a reference frame moving with the pump pulse, where $\Delta\beta_1 = \beta_{12} - \beta_{11}$ accounts for the group-velocity mismatch between the pump and probe pulses. Here, $\beta_{mn} = d^m\beta_n/d\omega^m$, with $n = 1$ and 2 for the pump and probe, respectively, are various dispersion parameters. In particular, β_{21} and β_{22} are the group-velocity dispersion (GVD) parameters at the pump and probe wavelengths, respectively. Losses are included only in the pump equation through α as the pump intensity significantly impacts the probe evolution, while the probe intensity plays a minor role. The nonlinear parameter is defined as $\gamma_j = 2\pi n_2/(\lambda_j A_{\text{eff}})$, where λ_j is the wavelength, n_2 is the Kerr coefficient (units of m^2/W), and A_{eff} is the effective mode area of the waveguide assumed to support a single mode [3]. Although different γ 's must be used when pump and probe wavelengths are far apart, here we assume that the two wavelengths are close enough that $\gamma_1 \approx \gamma_2 = \gamma$. Several higher-order effects are not included in Eqs. (1) and (2). For example, we ignore the third- and higher-order dispersion terms. We also neglect the shock and Raman terms that play important roles for ultrashort pulses. We justify their omission by focusing on relatively long pulses (>3 ps) with relatively low peak powers (<5 W).

In a standard approach used in nearly all XPM studies, Eqs. (1) and (2) are solved numerically with the split-step Fourier method to study pump-induced spectral changes in the shape and spectrum of a probe pulse. Here the same two equations are used to study the phenomena of temporal reflection and refraction from a pump pulse; however, one must

choose the pulse parameters judiciously to observe these phenomena. Our past work [26] has shown that the pump and probe pulses have similar group velocities (i.e., $\Delta\beta_1$ should not be too large) for significant reflection to occur. One way to have similar group velocities is to ensure that the wavelength difference $\Delta\lambda$ between the pump and probe is relatively small. However, since the pump spectrum broadens through self-phase modulation (SPM), $\Delta\lambda$ must be large enough that probe spectrum does not overlap with it. Moreover, $\Delta\lambda$ must be large enough that the probe is outside the parametric gain bandwidth of any four-wave mixing process. In the following we consider two practical scenarios. In each case, we use parameter values that are either realistic for commercial fibers or can be realized using custom-designed fibers.

A. Super-Gaussian Pump Pulses

In a practically relevant case, we choose the center wavelength of the pump pulse such that it coincides with the zero-dispersion wavelength of the fiber ($\beta_{22} = 0$). In this case, the shape of the pump pulse will not change during propagation, creating an unchanging boundary in time. To ensure a sharp temporal boundary, we assume a super-Gaussian shape for the pump pulse in the form

$$A_1(0, t) = \sqrt{P_1} \exp\left[-\frac{1}{2}\left(\frac{t - T_d}{T_{01}}\right)^{2m}\right], \quad (3)$$

where P_1 is the peak power, T_d is a relative delay between the pump and probe pulses, and T_{01} is the $1/e$ width of the pump. The integer m affects the rise and fall times of the pulse wings; $m = 4$ was chosen to produce a relatively sharp temporal boundary. The shape of the probe pulse is not critical for the results presented here. We use a Gaussian shape of the form

$$A_2(t) = \sqrt{P_2} \exp\left[-\frac{1}{2}\left(\frac{t}{T_{02}}\right)^2\right], \quad (4)$$

where P_2 is the peak power and T_{02} is the $1/e$ width of the probe. P_2 is kept small enough that the probe does not influence its own spectrum through SPM.

Figure 1 shows the evolution of the pulse shape (left) and spectrum (right) for the probe (top) and pump (bottom) pulses. The parameter values used for the fiber were $\beta_{21} = 0$, $\Delta\beta_1 = 31.4$ ps/km, $\beta_{22} = 25$ ps²/km, $\alpha_{\text{dB}} = 0.3$ dB/km, and $\gamma = 2$ W⁻¹/km. The pump and probe pulses had parameters $T_{01} = 20$ ps, $T_{02} = 10$ ps, $T_d = 50$ ps, $P_1 = 5$ W, and $P_2 = 1$ mW. For the long duration pulses used here, we can safely neglect β_3 for probe pulses as even a relatively high value of $\beta_3 = 1$ ps³/km gives a third-order dispersion length of $L_{D,3} > 150$ km, much larger than the 3-km length of the fiber used for Fig. 1. The pump pulse may be affected by higher-order dispersion because of its relatively sharp edges. However, our pump pulses are so wide that even the fourth-order dispersion plays a minor role for them.

The behavior of the pump pulse is easy to understand. Because $\beta_{21} = 0$, it propagates without any change in its shape, even though its spectrum broadens significantly as a result of SPM. The behavior of the probe pulse exhibits unique features both in time and frequency that can be understood as a temporal reflection of the probe after it arrives at the temporal boundary created by the pump pulse. As the probe pulse crosses

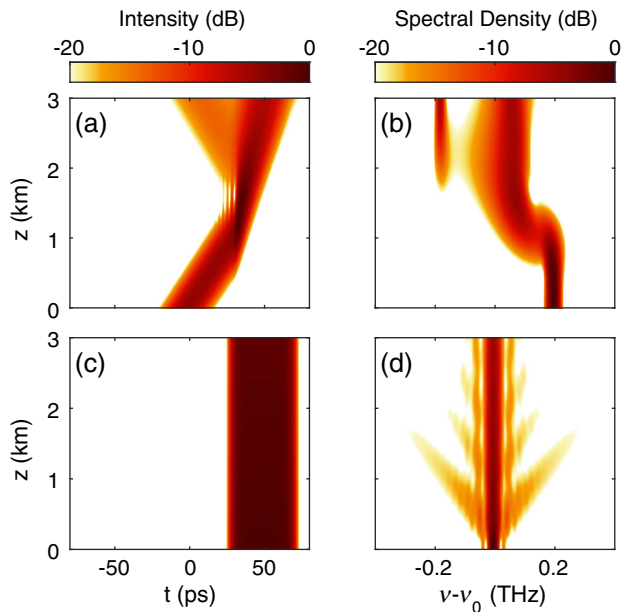


Fig. 1. Temporal (left column) and spectral (right column) evolutions over a 3-km-long fiber for the probe [(a), (b)] and pump [(c), (d)] pulses. The pump pulse has a super-Gaussian shape and propagates at the zero-dispersion wavelength of the fiber. (See text for other parameter values.) The time axis is measured in a reference frame that is moving with the pump pulse such that $t - T - z/v_{g1}$.

the leading edge of the pump, it undergoes reflection and refraction, splitting into two distinct parts whose spectra undergo different amounts of spectral shifts. Note that the changing pump spectrum has no influence on the reflection process. The only important factor is the temporal profile of the pump pulse. The reason is obvious once one realizes that the XPM depends on the intensity of the pump and not on its phase.

One may ask how the results in Fig. 1 differ from our past work where the temporal boundary was assumed to be infinitely sharp [26]. An obvious difference is that the shifting and splitting of the spectrum happens over a much longer distance. As seen in Fig. 1(b), the spectrum of the transmitted pulse has redshifted after 1 km, but the reflected spectrum with a much larger redshift appears only after 1.5 km. This is clearly due to a finite rise time of the pump's leading edge, which causes the probe pulse to gradually pass through an increasing refractive-index change before arriving at the final shift when $t = T_d$. At the early part of this process, changes in the refractive index are too small for reflection to occur. However, as the pump power quickly ramps up, more of the probe energy is reflected.

In the case of an infinitely sharp temporal boundary, the spectral shifts for the reflected and refracted pulses can be found analytically in the form [26]

$$\Delta\omega_r = -\Delta\omega_i, \quad \Delta\omega_t = \Delta\omega_i \sqrt{1 - \frac{4\gamma P_1 \beta_{22}}{(\Delta\beta_1)^2}}, \quad (5)$$

where all shifts are relative to the frequency ω_c at which $v_g(\omega_c) = v_{g1}$, i.e., $\Delta\omega = \omega - \omega_c$. Here $\Delta\omega_r$ is the reflected center frequency and $\Delta\omega_t$ is the transmitted center frequency.

It follows from the reflection condition that $\omega_c = (\omega_i + \omega_r)/2$, where ω_r is the center frequency of the reflected part. Similarly, ω_t is the center frequency of the transmitted part. Using the parameter values from Fig. 1, we conclude that the predictions of Eq. (5) agree reasonably well with the numerical results.

We stress that temporal reflection seen in Figs. 1 and 2 cannot be explained as a four-wave mixing (FWM) process because Eqs. (1) and (2) contain only the SPM and XPM terms and forbid any energy exchange between the pump and probe pulses. We are aware that reflection of a weak probe from a soliton has been interpreted as a FWM-like process in the past [32,33]. Recall that FWM is a four-photon process in which pump energy is used to create the idler at a new frequency and to amplify the probe simultaneously. In the case of the temporal reflection studied here, no pump energy is lost and no probe amplification occurs. Rather, the probe phase is modulated by the pump through XPM, and a part of probe energy undergoes spectral shift. SPM of the pump plays virtually no role in this process. Indeed, if we remove the SPM terms in Eq. (1) that are critical for solitons, the behavior of the probe does not change in the top row of Fig. 1.

One can ask what happens if the peak power of the probe pulses is increased. When XPM is used to create a temporal boundary, the energy lost or gained from the probe must be transferred to or from the pump. Indeed, if the peak power P_2 is increased, the probe pulse still undergoes reflection at the edge of the pump, but the pump spectrum is blueshifted to compensate for the redshift of the reflected and transmitted pulses. Increasing the probe-pulse energy by increasing the pulse width T_{02} while maintaining the peak power also results in a larger shift of the pump frequency. Of course, the blueshifts of the pump can also be interpreted as phase modulation of the pump by the probe pulse.

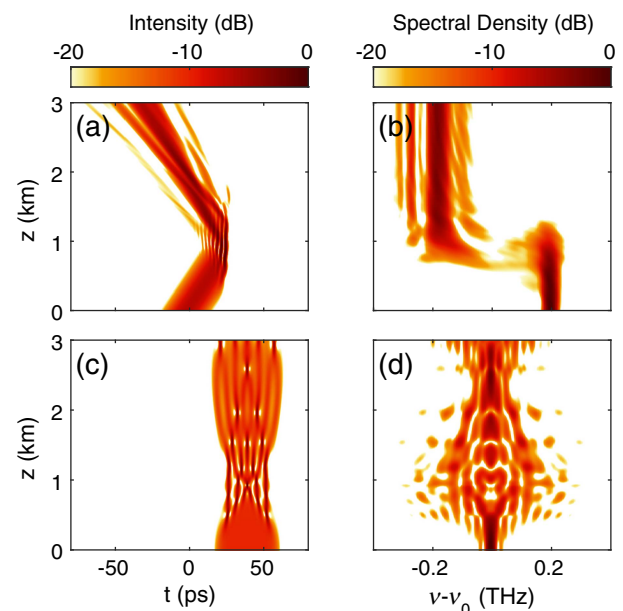


Fig. 2. Same as Fig. 1 except the GVD of the pump was changed to $\beta_{21} = -25 \text{ ps}^2/\text{km}$.

Dispersive broadening of the pump pulse can also be avoided if it propagates in the anomalous-dispersion regime of the fiber. To keep the group velocities nearly the same, the probe pulse must be on the opposite side of the zero-dispersion wavelength of the fiber, i.e., the pump and the probe must have opposite GVD signs. We assume that the wavelength difference between the pump and probe is still not too large, but this assumption can easily be relaxed. Figure 2 shows numerical simulations under conditions identical to those of Fig. 1, except that the pump GVD is not zero and is set to $\beta_{21} = -25 \text{ ps}^2/\text{km}$ and the initial delay is reduced to $T_d = 40 \text{ ps}$. A direct comparison shows that the behavior of both pulses in Fig. 2 is markedly different from that in Fig. 1. The pump pulse now breaks down into multiple shorter pulses, which cause the probe to see a larger refractive-index change compared to the nondispersive case. As a result, the probe pulse is now entirely reflected at the edge of the pump, and nearly all probe energy is transferred to a new redshifted spectral band. Moreover, additional side bands appear because the pump pulse narrows in time as it propagates, causing the refractive-index boundary to recede toward the center of the pump pulse. This causes the boundary to move at a different velocity, which leads to different reflected and transmitted frequencies.

If the sign of the GVD parameter of the pump is reversed, normal dispersion causes the pump pulse to spread out in time. By the time the probe pulse catches up with the pump, the peak power of the pump is significantly reduced, resulting in much smaller changes in the refractive index. At the same time, the temporal boundary created by the pump pulse loses its sharpness. As a result, the reflected pulse is almost entirely suppressed owing to the slow rise time of the refractive index boundary. Experimentally, one could compensate for this by using a pump pulse that has been initially chirped with the opposite dispersion. This causes the pump to compress before the probe arrives, leading to a sharp boundary and allowing reflection to occur.

B. Soliton-Shaped Pump Pulses

The reason that the pump pulse in Fig. 2(a) breaks down into multiple shorter pulses with very high peak powers is related to the onset of modulation instability occurring in the case of anomalous dispersion [3]. Since optical solitons can also form under such conditions, a simple solution to avoid the breakdown and broadening of the pump pulse is to launch the pump pulse so that it propagates in the form of a fundamental soliton. While this limits the pump to the anomalous-dispersion regime, the shape and width of the pump pulse will not change during propagation, providing a shape-invariant moving boundary. To study reflections from such a boundary, the input field of the pump pulse is taken to be

$$A_1(0, t) = \sqrt{P_1} \text{sech}\left(\frac{t - T_d}{T_{01}}\right). \quad (6)$$

Unlike the Gaussian pump, the peak power and width of the soliton are linked through the relation

$$P_1 = \frac{|\beta_{21}|}{\gamma T_{01}^2}. \quad (7)$$

Note that higher peak powers can be realized only by reducing the width of the soliton. In the following simulations, the

width of the pump pulse is chosen to be a fraction of that associated with the probe pulse.

For the sake of comparison, we use the same simulation parameters as in Fig. 2, except that the width of pump pulse is reduced to $T_{01} = 1.58 \text{ ps}$ to keep its peak power at 5 W . The pulse separation is also reduced to $T_d = 30 \text{ ps}$ so that the two pulses overlap at about the same distance. Figure 3 shows the evolution of the pump and probe pulses over 3 km of fiber length in this situation. As expected, the pump pulse forms a fundamental soliton and propagates without any change in its shape or spectrum. The probe pulse still undergoes reflection and refraction at the boundary. However, the spectrum of the transmitted pulse quickly returns to the incident frequency. This occurs because the transmitted pulse encounters a second boundary on the trailing side of the soliton and is refracted a second time. For this second refraction, the sign of the refractive-index change is reversed, so we return to the original frequency. Moreover, unlike the single refraction from the super-Gaussian pump pulse where the transmitted pulse is compressed in time, the width of the transmitted pulse remains nearly the same and its group velocity is unchanged.

The quick change back to the original frequency of the transmitted pulse has one final effect. During the reflection process, a temporal analog of the evanescent wave occurs, where a portion of the pulse energy extends past the boundary, even during TIR [26]. The soliton is so narrow in time that the evanescent wave extends from one side of the soliton to the other, allowing for a temporal analog of frustrated TIR. In other words, the reflected pulse in Fig. 3 is weaker than it should be. We verified this effect by increasing the peak power of the pump pulse such that the index change was large enough for TIR to occur in the case of a single ideal temporal boundary. Although most of the probe pulse was reflected, as expected, a small portion of probe energy tunneled through the trailing

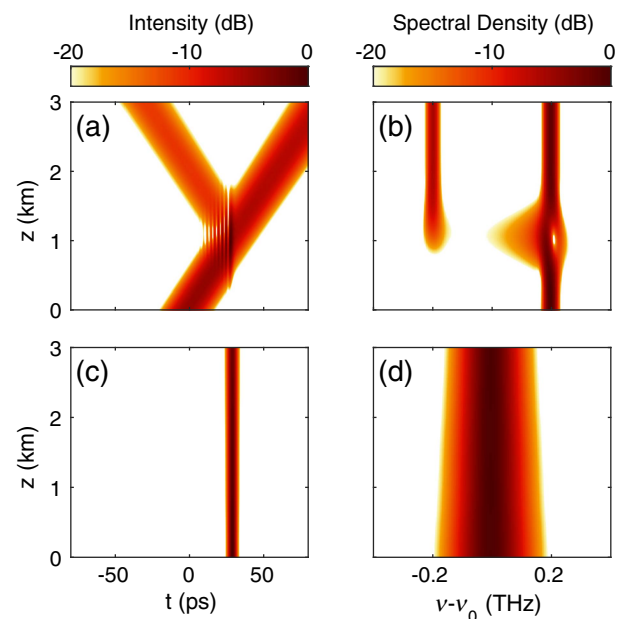


Fig. 3. Same as Fig. 2, except that the pump pulse propagates as a fundamental soliton with $T_{01} = 1.58 \text{ ps}$.

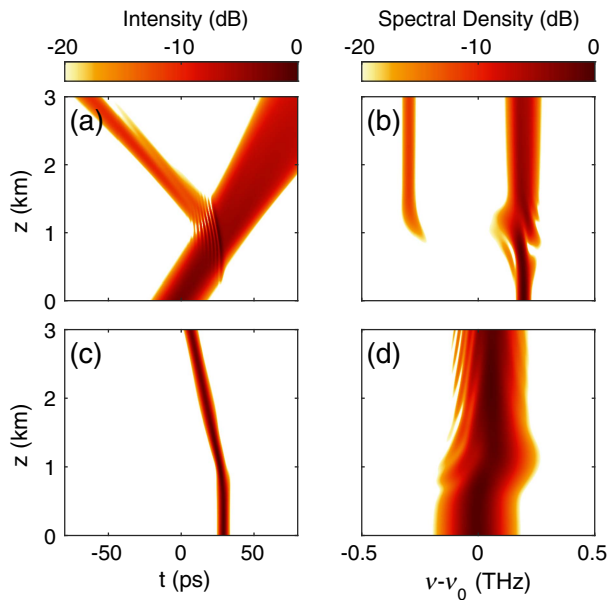


Fig. 4. Same as Fig. 3, except that the probe power has been increased to $P_2 = 1$ W.

edge of the soliton that acted as a second boundary. The frustrated TIR effect can be removed by increasing the pump width, which has a drastic effect on the tunneling probability. This dependence on the duration of the pump pulse explains why this effect was not seen for the 20-ps-wide super-Gaussian pump pulse used in Fig. 1. Looking at Eq. (7), the frustrated TIR effect can be reduced using a pump wavelength with a higher GVD, which can accommodate a wider soliton while still having the same peak power.

If we increase the peak power of the probe pulse, we expect the frequency of the soliton to change because of the probe-induced XPM effects on the pump pulse. Figure 4 shows the results using the same parameters as in Fig. 3 but with the probe power increased to $P_2 = 1$ W. As seen in Fig. 4(d), the soliton frequency shifts by ~ 0.1 THz toward the blue side. Because of the pump's GVD, this frequency shift causes the soliton to speed up, as indicated by the leftward tilt of the soliton trajectory in Fig. 3(c). The blue shift of the soliton also affects the probe pulse by changing the speed of the temporal boundary. More specifically, the momentum conservation condition at the boundary changes after the blueshift. This leads to an additional redshift of the reflected pulse at a distance of about 1 km, as seen clearly in Fig. 4(b).

3. TEMPORAL WAVEGUIDES

In our earlier work [30], we analyzed a temporal waveguide made with two sharp temporal boundaries inside which the refractive index was different from the outside region. We found that such a waveguide supports one or more temporal modes in close analogy with the spatial planar waveguides. We also defined a dimensionless waveguide parameter as

$$V = 2\sqrt{\frac{-(\Delta n)\beta_0 T_B^2}{\beta_2}}, \quad (8)$$

where Δn is the index change inside the core region, β_0 is the propagation constant, and T_B is the width of the core region of the waveguide. Just like its spatial counterpart, this parameter governs the number of modes supported by the temporal waveguide. A temporal mode is no longer supported when $V < m\pi/2$, where $m = 0, 1, 2, \dots$ is the mode order. In particular, only a single temporal mode can propagate inside the waveguide when $V < \pi/2$. Notice that V is real only if Δn and β_2 have opposite signs. In particular, when $\beta_2 > 0$ (normal dispersion), the refractive index inside the core region should be smaller than that outside of it. This situation does not occur in spatial waveguides that always require Δn to be positive.

Because the Kerr nonlinearity causes only a positive change in the refractive index ($\Delta n > 0$), the probe must experience a GVD such that V is real. There are only two possible methods for creating a temporal waveguide through XPM. The first is to place the probe pulse at the center of a relatively wide pump pulse such that the entire pump pulse acts as the core of a temporal waveguide that confines the probe pulse inside of it. To have a real V , this method requires that the probe wavelength be located in the anomalous-dispersion region ($\beta_2 < 0$). The second method places the probe in the normal-dispersion region ($\beta_2 > 0$) and uses two short pump pulses that act as the waveguide boundaries so that Δn is negative inside the core region. In any other arrangement, the pump will actually act as an anti-waveguide.

When a single pump pulse is used to create the core region, the situation becomes qualitatively different because the waveguide is a graded-index type (rather than a step-index type). Moreover, the shape and width of the core region will change during propagation if the pump pulse spreads through the dispersive effects. We can avoid pump broadening if the pump pulse forms a fundamental soliton, but this approach presents its own unique challenges. As was done in Section 2, we consider pump pulses whose shapes are either super-Gaussian (or Gaussian) or correspond to that of a soliton.

A. Gaussian or Super-Gaussian Pump Pulses

We first use Gaussian shapes for both the pump and probe pulses [$m = 1$ in Eq. (4)] but assume that the pump is no longer delayed with respect to the probe ($T_d = 0$). The probe is chosen to be temporally narrower than the pump and is placed in the middle of the pump at $t = 0$. Because XPM increases the refractive index inside the pump region, Δn is positive inside the core region. It follows from Eq. (8) that the probe pulse must experience anomalous GVD ($\beta_{22} < 0$). As before, the behavior of the pump pulse depends on the sign of GVD parameter β_{21} at its wavelength. In particular, the pump pulse will remain nearly unchanged if its wavelength coincides with the zero-dispersion wavelength of the fiber.

Figure 5 shows the evolution of the pump and probe in the specific case of $\beta_{21} = 0$. The other parameter values were $\Delta\beta_1 = 0$ ps/km, $\beta_{22} = -25$ ps²/km, $\gamma = 2(\text{W})^{-1}/\text{km}$, $T_{01} = 2.5$ ps, $T_{02} = 1$ ps, $T_d = 0$ ps, $P_1 = 1$ W, and $P_2 = 1$ mW. We have verified that the higher-order dispersive and nonlinear effects are negligible even for such pump pulses. As before, the pump pulse does not change shape during propagation, while its spectrum changes owing to SPM.

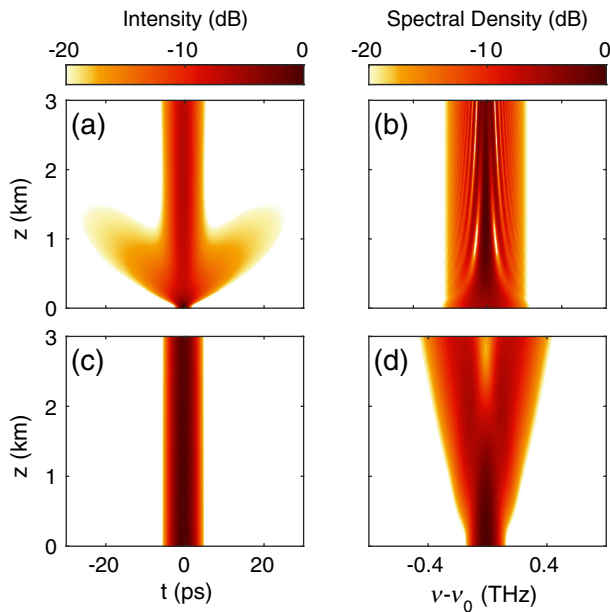


Fig. 5. Temporal (left column) and spectral (right column) evolutions over a 3-km-long fiber for the probe [(a), (b)] and pump [(c), (d)] pulses. The pump pulse has a Gaussian shape and is propagating at the zero-dispersion wavelength of the fiber. (See text for other parameter values.)

The evolution of the probe pulse is much more interesting. Even though it sheds some energy initially in the region outside the pump pulse, it propagates without any changes in its shape or width. This is remarkable since the probe pulse would broaden by a factor of 100 over a length of 3 km in view of its 40-m dispersion length calculated using $L_D = T_{02}^2/|\beta_{22}|$. Since the probe pulse remains confined within the pump pulse, we interpret it as XPM-induced temporal waveguiding of the probe by the pump. Indeed, the evolution seen in Fig. 5(a) is similar to what one would observe in a single-mode spatial waveguide when the input beam shape does not coincide with the spatial shape of the waveguide mode. In our case, the Gaussian shape of the probe is different from the temporal shape of the waveguide mode. As a result, the probe sheds some energy initially as it adjusts its shape but then is guided by the pump pulse and remains trapped inside it. If we use the relations $\beta_0 \Delta n = 2\gamma P_1$ and $T_B = T_{01}$ in Eq. (8), we find that the XPM-induced waveguide is in fact a single-mode waveguide with $V = 1.41$.

If the probe pulse is in a region with normal dispersion, the refractive index outside of the waveguide must be greater than the refractive index inside of the waveguide. Therefore, the waveguide must be formed by two pump pulses, with the waveguide occupying the region between them. Figure 6 shows numerical simulations under the conditions of Fig. 5 but with two super-Gaussian pump pulses separated by 12 ps. Even though the two pulses overlap to some extent, the central region between them has a slightly smaller index change, making effective Δn negative inside the core region. This scheme has the added advantage that the number modes supported by the waveguide can be altered simply by changing the spacing between the two pump pulses.

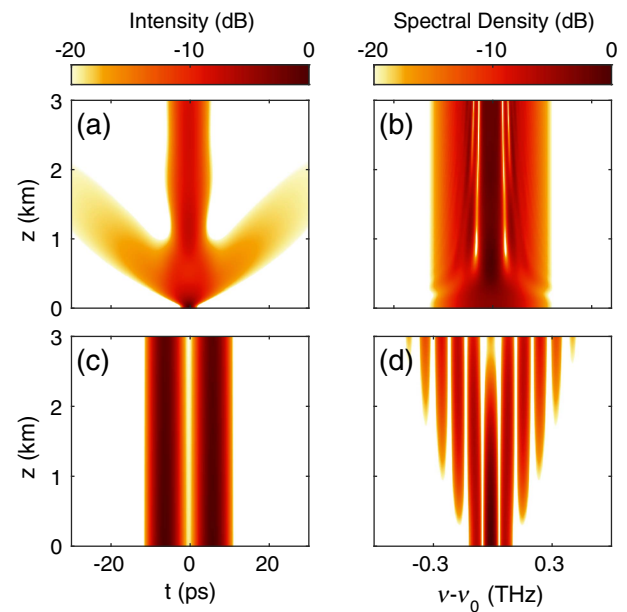


Fig. 6. Same as Fig. 5, except that the temporal waveguide is formed by using two super-Gaussian pump pulses separated by 12 ps.

If the pump pulse is not at the zero-dispersion wavelength, the GVD will cause the pump shape to change, which, in turn, will cause the waveguide to broaden in the case of the single-pump configuration and to collapse entirely with the two-pump configuration. While some GVD can be tolerated at the pump wavelength, the corresponding probe GVD should be higher to allow the probe pulse to fill the waveguide before the pump disperses. This ends up creating essentially the same behavior as the zero-GVD situation. In the case of normal GVD at the pump wavelength ($\beta_{21} > 0$), we can compensate for pump broadening by first chirping the pump with the opposite dispersion before propagating it with the probe pulse. This allows the pump to compress during propagation, although the probe pulse will lose some of its energy initially before the waveguide is formed. This method is less effective for waveguides formed by two pump pulses since the two dispersed pulses interfere with one another to form a more-complex temporal profile when they are dispersed. However, it will work for sufficiently wide temporal waveguides as long as the two dispersed pump pulses do not overlap in time.

A simpler solution exists when we have anomalous pump dispersion since the pump pulse chirps itself through SPM in such a way that the waveguide shape will be preserved for a longer distance. Figure 7 shows the evolution for the same parameters as Fig. 5 but with GVD $\beta_{21} = -25$ ps²/km and the pump power increased to $P_1 = 2$ W. As shown in Fig. 7(c), the pump pulse broadens initially, but SPM prevents further broadening. This allows the XPM-induced waveguide to persist over the entire propagation distance. A comparison with Fig. 5 shows that the probe pulse is trapped in nearly the same way as the zero-GVD case. Note that the pump pulse in Fig. 7(c) can be thought to be evolving toward a soliton. We next examine the behavior when the pump is simply launched as a fundamental soliton.

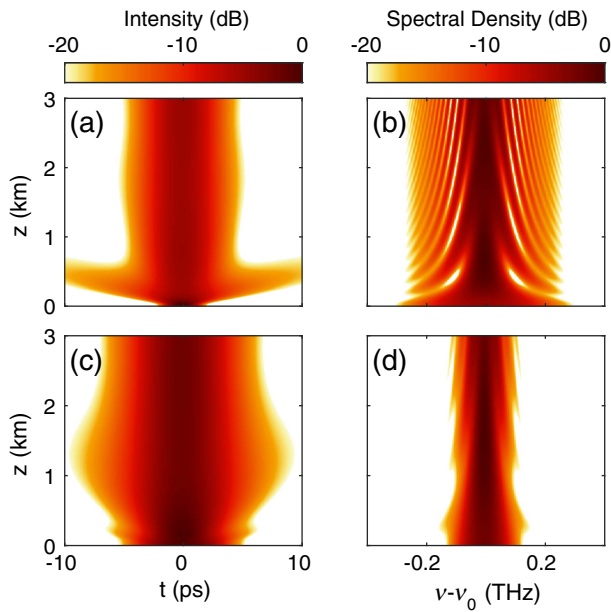


Fig. 7. Same as Fig. 5, except that the temporal waveguide is formed by a single super-Gaussian pump propagating in the anomalous-GVD region.

B. Soliton-Shaped Pump Pulses

As seen earlier, the width of a soliton and its peak power are linked. If we use the relation $\beta_0 \Delta n = 2\gamma P_1$ together with Eq. (7) for P_1 to calculate the V parameter in Eq. (8), we find that a soliton waveguide has a V parameter of the form

$$V = 2\sqrt{\frac{|\beta_{21}| T_B^2}{|\beta_{22}| T_{01}^2}} \quad (9)$$

We stress that this relation is not exact since the soliton has a finite rise time. It is, however, a useful tool for approximating how many modes the waveguide should support.

We will now examine the case where the waveguide is formed by a single soliton pulse. In this case, the half-width of the waveguide (T_B) is approximately equal to T_{01} , and Eq. (9) reduces to

$$V \approx 2\sqrt{\frac{|\beta_{21}|}{|\beta_{22}|}} \quad (10)$$

Consequently, the number of modes supported by the waveguide is almost entirely determined by the ratio of the GVD parameters at the pump and probe frequencies. Note that the width and peak power of the pump are not constrained, so the waveguide can be constructed for any pulse width. The modes will simply scale their widths and spectra up or down to match the waveguide.

Figure 8 shows the evolution of probe pulses with $T_{02} = 5$ ps and a GVD of $\beta_{21} = \beta_{22} = -25$ ps²/km at two pump powers of [(a), (b)] $P_1 = 1$ W and [(c), (d)] $P_1 = 0.2$ W. These pump powers create waveguides that are about 7 ps and 15.8 ps wide, respectively. Because the GVD values are the same at the pump and probe, the V parameter is approximately 2 in both cases. As the probe pulse evolves, however, it seems to excite

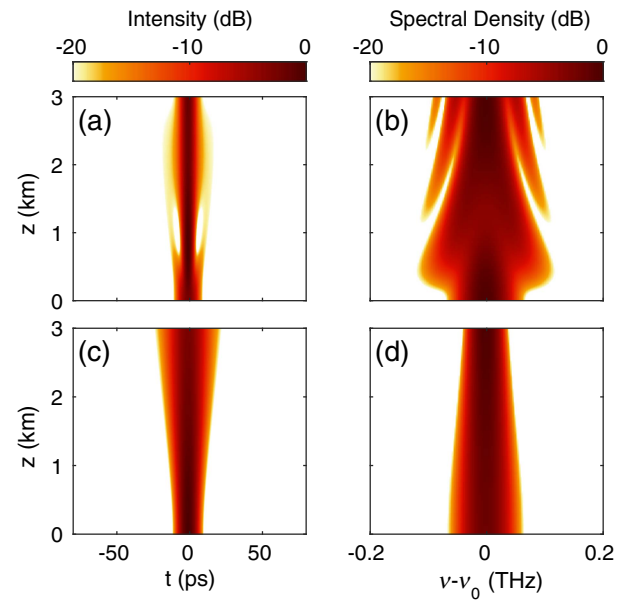


Fig. 8. Evolution of pulse shape [(a), (c)] and spectrum [(b), (d)] for a Gaussian probe pulse in a waveguide formed by a single soliton with $P_1 = 1$ W (top) and $P_1 = 0.2$ W (bottom).

only one mode. This is not too surprising in view of the approximate nature of Eq. (9). One more feature is noteworthy: even though the waveguide width changes in the top and bottom rows of Fig. 8, the peak power of the soliton also changes in such a way that the waveguide mode is preserved. This also makes intuitive sense since the soliton is essentially producing its own waveguide.

If the temporal waveguide is formed by using two solitons, we can set the waveguide width arbitrarily through spacing between them and can therefore control the number of modes supported by the waveguide. If we wish to have a highly multi-mode waveguide, we can increase either the power of the solitons or their separation. If we seek a single-mode waveguide, however, we begin to run into the problem of soliton attraction and repulsion. In this process, solitons that are close together in time will either pull together or push apart depending on the relative phase between the two pulses. In either case, the waveguide will eventually break down by either collapsing or widening until it once again supports multiple modes. As before, we can avoid the interaction issue by using a pump wavelength that has a low GVD relative to the probe GVD. This forces the V parameter to be small, allowing for single-mode operation. Another solution is to launch the two solitons with an initial relative phase shift of $\pi/4$. In this case, the solitons neither repel nor attract one another, leading to a more stable waveguide.

As seen in Fig. 4, the energy in the probe pulse can have a significant effect on the group velocity of the soliton. For a waveguide formed by two solitons, the group velocity of the leading soliton decreases as energy is transferred from the soliton to the probe, while the group velocity of the trailing soliton increases as energy is transferred from the probe to the soliton. If the energy in the probe pulse is increased further, these two solitons will collide and cause the waveguide to collapse. On the

other hand, for a waveguide formed by a single soliton, the leading and trailing edges are formed by the same soliton. Because the soliton gains energy at the trailing edge and loses energy at the leading edge, the net effect is that the soliton frequency stays the same and the temporal waveguide is maintained.

4. PULSE JITTER COMPENSATION

If two pulsed laser sources have synchronized repetition rates, some jitter may still remain in the timing of the two overlapping pulses at different wavelengths. This interpulse jitter manifests as a randomly varying delay between the centers of the two pulses. The concept of XPM-induced temporal waveguiding discussed in this paper provides a potential mechanism for removing such timing jitter. One of the pulsed lasers acts as the pump, while the other laser provides the probe pulses. The temporal waveguide created by the pump pulse guides the probe pulse inside it and reduces the interpulse jitter for the following reason: if a probe pulse is displaced from the waveguide center because of the jitter, it will shed some energy and reshape itself to match the shape of the fundamental mode supported by the temporal waveguide. A larger displacement leads to higher energy loss, effectively converting the timing jitter into amplitude jitter.

Our numerical simulations confirm the preceding scenario. Figure 9 shows the evolution of three identical probe pulses ($T_{02} = 5$ ps), except that the probe is displaced from the waveguide center by (a) 0 ps, (b) 2 ps, and (c) 4 ps. In all three cases, probe pulses are propagating inside an 8-ps-wide temporal waveguide formed by two super-Gaussian pump pulses with $T_{01} = 4$ ps, $m = 2$, and $P_1 = 1.6$ W. The pump pulses propagate in the region of anomalous dispersion with $\beta_{21} = -10$ ps²/km, while the probe pulses see normal GVD with

$\beta_{22} = 60$ ps²/km to ensure that they fill the waveguide quickly. The output pulse shapes are shown in Fig. 9(d), where it is evident that although the probe pulses start with different offsets, they lose some energy outside of the waveguiding region and eventually shift their peak position such that it is located in the center of the temporal waveguide.

Examining the output pulse shapes in Fig. 9(d), we note that larger time offsets lead to a larger reduction in the peak power of the probe pulse since more energy is lost to the region outside of the waveguide as the pulse adjusts its shape to match the shape of the waveguide mode. Clearly, the timing jitter of the pulses has been traded with an amplitude jitter. Although not desirable, amplitude jitter may be more acceptable than the timing jitter for some applications. Note also that for offsets of less than 2 ps, the reduction in peak power is relatively small. This means that the XPM-induced waveguide can compensate for jitter of nearly half the pulse width without significantly altering the peak power of the probe pulses. We note that the jitter compensation is not fully complete after the 8 km of fiber, although the maximum offset from the waveguide center is reduced by nearly a factor of 8 to <0.5 ps. A longer fiber length should lead to better jitter compensation, though fiber losses will begin to degrade the temporal waveguide.

The fiber length needed to reduce the jitter depends on the pulse widths. If the two pulse trains contain shorter femtosecond pulses, the required fiber length would be much smaller than the one in Fig. 9. This is because shorter probe pulses have a shorter dispersion length and therefore can fill the waveguide after a smaller distance. However, the higher-order dispersive and nonlinear effects, not included here, must be taken into account for such pulses.

5. CONCLUSIONS

Cross-phase modulation is commonly viewed as a nonlinear process that chirps a probe pulse and modifies its spectrum when an intense pump pulse overlaps with it. Here we present an alternative view of XPM in which the pump pulse creates a moving refractive-index boundary that splits the probe pulse into two parts with distinct optical spectra through temporal reflection and refraction inside a dispersive nonlinear medium. The probe even undergoes a temporal version of TIR for sufficiently intense pump pulses, a phenomenon that can be exploited for making temporal waveguides.

Through numerical simulations, we have investigated the practical conditions under which the nonlinear phenomenon of XPM, implemented with a pump-probe configuration, can be used to observe temporal reflection and refraction as well as to form a temporal waveguide. Since the moving temporal boundaries are produced by the leading and trailing edges of the pump pulse, its shape plays a critical role. Moreover, the boundaries can change during propagation because of the GVD at the pump wavelength. One solution is to choose the pump wavelength to coincide with the zero-dispersion wavelength of the waveguide used and choose a super-Gaussian shape for pump pulses that have relatively sharp edges. This configuration has been discussed here in detail.

Another important configuration chooses the pump wavelength such that the GVD is negative. In this case, a relatively

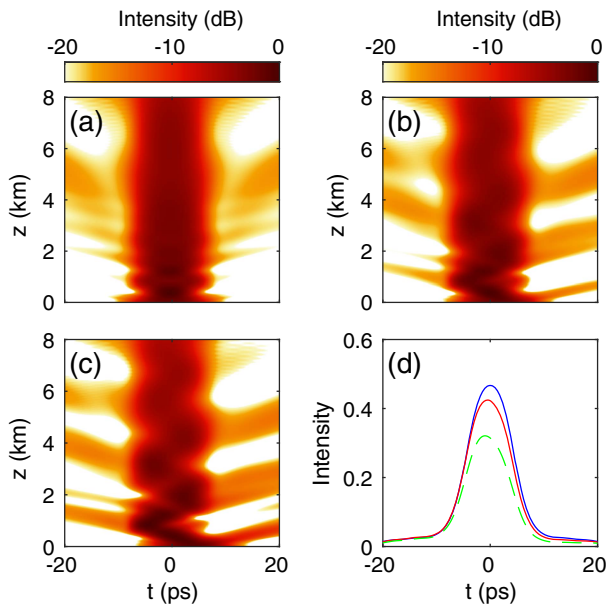


Fig. 9. Evolution of three probe pulses that are offset from the waveguide center by (a) 0 ps, (b) 2 ps, and (c) 4 ps. Temporal waveguide is created through XPM by two pump pulses separated by 8 ps. (d) The output shapes of three probe pulses are shown.

wide pump pulse can form a higher-order soliton that breaks into multiple narrower and more-intense pulses and results in a much larger refractive-index change than the original pulse could provide. Our results show that the probe pulse experiences a temporal version of TIR under such conditions. Of course, the pump parameters can also be adjusted such that it propagates as a fundamental soliton. We found that if the soliton width is relatively narrow, the trailing edge of the soliton can lead to frustrated TIR and some probe energy will leak to the back side of the soliton.

In this paper we used relatively wide picosecond pulses to examine the underlying physics as simply as possible. If shorter femtosecond pulses are employed, Eqs. (1) and (2) should be replaced with their generalized versions that include all higher-order dispersive and nonlinear effects including intrapulse Raman scattering, which shifts the pump spectrum toward longer wavelengths [3]. This frequency shift would change the speed of the pump pulse relative to the probe pulse and therefore modify the reflected and transmitted frequencies. If multiple pump pulses are used to form a temporal waveguide, such spectral shifts could also lead to a collapse of the waveguide. In addition, higher-order dispersion effects would cause the pump pulse shape to change significantly. For all these reasons, we feel that picosecond pulses are preferable for experiments.

Our numerical simulations provide a basis for an experimental demonstration of temporal reflection using XPM. The soliton-induced boundaries are perhaps the simplest to implement in practice. If a commercial, dispersion-shifted, telecommunication fiber is used with its zero-dispersion wavelength near 1500 nm, one can employ intense pump pulses near 1550 nm and probe pulses near 1450 nm. The fiber length of 3 km was chosen to allow the reflected and refracted pulses to separate in time. This distance can be reduced to around 1.5 km, and could be reduced even further if somewhat shorter pulses are employed. Another possibility is to launch pump pulses at the zero-dispersion wavelength itself and probe pulses near 1550 nm. In general, the use of XPM requires careful consideration of the materials' dispersive properties. If a photonic crystal fiber is used for observing the effects discussed here, Eqs. (1) and (2) should be modified to take into account the actual dispersion characteristics of such fibers.

Funding. National Nuclear Security Administration (NNSA) (DE-NA0001944); University of Rochester (UR); New York State Energy Research and Development Authority (NYSERDA); National Science Foundation (NSF) (ECCS-1505636).

Acknowledgment. This material is based upon work supported by the Department of Energy National Nuclear Security Administration, the University of Rochester, the New York State Energy Research and Development Authority, and the National Science Foundation. This report was prepared as an account of work sponsored by an agency of the U.S. Government. Neither the U.S. Government nor any agency thereof, nor any of their employees, makes any warranty, express or implied, or assumes any legal liability or responsibility

for the accuracy, completeness, or usefulness of any information, apparatus, product, or process disclosed, or represents that its use would not infringe privately owned rights. Reference herein to any specific commercial product, process, or service by trade name, trademark, manufacturer, or otherwise does not necessarily constitute or imply its endorsement, recommendation, or favoring by the U.S. Government or any agency thereof. The views and opinions of authors expressed herein do not necessarily state or reflect those of the U.S. Government or any agency thereof.

REFERENCES

1. R. W. Boyd, *Nonlinear Optics* (Academic, 2003).
2. K. Okamoto, *Fundamentals of Optical Waveguides*, 2nd ed. (Academic, 2006).
3. G. P. Agrawal, *Nonlinear Fiber Optics*, 5th ed. (Elsevier, 2013).
4. A. V. Gorbach and D. V. Skryabin, "Bouncing of a dispersive pulse on an accelerating soliton and stepwise frequency conversion in optical fibers," *Opt. Express* **15**, 14560–14565 (2007).
5. S. Robertson and U. Leonhardt, "Frequency shifting at fiber-optical event horizons: the effect of Raman deceleration," *Phys. Rev. A* **81**, 063835 (2010).
6. A. Demircan, S. Amiranashvili, and G. Steinmeyer, "Controlling light by light with an optical event horizon," *Phys. Rev. Lett.* **106**, 163901 (2011).
7. E. Rubino, A. Lotti, F. Belgiorno, S. L. Cacciatori, A. Couairon, U. Leonhardt, and D. Faccio, "Soliton-induced relativistic-scattering and amplification," *Sci. Rep.* **2**, 932 (2012).
8. L. Tartara, "Frequency shifting of femtosecond pulses by reflection at solitons," *IEEE J. Quantum Electron.* **48**, 1439–1442 (2012).
9. S. Pickartz, U. Bandelow, and S. Amiranashvili, "Adiabatic theory of solitons fed by dispersive waves," *Phys. Rev. A* **94**, 033811 (2016).
10. T. G. Philbin, C. Kuklewicz, S. J. Robertson, S. Hill, F. König, and U. Leonhardt, "Fiber-optical analog of the event horizon," *Science* **319**, 1367–1370 (2008).
11. F. Belgiorno, S. L. Cacciatori, M. Clerici, V. Gorini, G. Ortenzi, L. Rizzi, E. Rubino, V. G. Sala, and D. Faccio, "Hawking radiation from ultrashort laser pulse filaments," *Phys. Rev. Lett.* **105**, 203901 (2010).
12. E. Rubino, F. Belgiorno, S. L. Cacciatori, M. Clerici, V. Gorini, G. Ortenzi, L. Rizzi, V. G. Sala, M. Kolesik, and D. Faccio, "Experimental evidence of analogue Hawking radiation from ultrashort laser pulse filaments," *New J. Phys.* **13**, 085005 (2011).
13. D. Faccio, "Laser pulse analogues for gravity and analogue Hawking radiation," *Contemp. Phys.* **53**, 97–112 (2012).
14. D. Faccio, T. Arane, M. Lamperti, and U. Leonhardt, "Optical black hole lasers," *Class. Quantum Grav.* **29**, 224009 (2012).
15. A. Shipulin, G. Onishchukov, and B. A. Malomed, "Suppression of soliton jitter by a copropagating support structure," *J. Opt. Soc. Am. B* **14**, 3393–3402 (1997).
16. R. Driben, A. V. Yulin, A. Efimov, and B. A. Malomed, "Trapping of light in solitonic cavities and its role in the supercontinuum generation," *Opt. Express* **21**, 19091–19096 (2013).
17. A. Demircan, S. Amiranashvili, C. Brée, U. Morgner, and G. Steinmeyer, "Supercontinuum generation by multiple scatterings at a group velocity horizon," *Opt. Express* **22**, 3866–3879 (2014).
18. J. Steinhauer, "Observation of self-amplifying Hawking radiation in an analogue black-hole laser," *Nat. Phys.* **10**, 864–869 (2014).
19. S. F. Wang, A. Mussot, M. Conforti, X. L. Zeng, and A. Kudlinski, "Bouncing of a dispersive wave in a solitonic cage," *Opt. Lett.* **40**, 3320–3323 (2015).
20. Z. Deng, X. Fu, J. Liu, C. Zhao, and S. Wen, "Trapping and controlling the dispersive wave within a solitonic well," *Opt. Express* **24**, 10302–10312 (2016).
21. S. C. Wilks, J. M. Dawson, W. B. Mori, T. Katsouleas, and M. E. Jones, "Photon accelerator," *Phys. Rev. Lett.* **62**, 2600–2603 (1989).
22. J. T. Mendonça, *Theory of Photon Acceleration*, Series in Plasma Physics (Institute of Physics Publishing, 2000).

23. J. T. Mendonça and P. K. Shukla, "Time refraction and time reflection: two basic concepts," *Phys. Scr.* **65**, 160–163 (2002).
24. F. Biancalana, A. Amann, A. V. Uskov, and E. P. O'Reilly, "Dynamics of light propagation in spatiotemporal dielectric structures," *Phys. Rev. E* **75**, 046607 (2007).
25. K. A. Lurie, "An introduction to the mathematical theory of dynamic materials," in *Advances in Mechanics and Mathematics*, D. Y. Gao and R. W. Ogden, eds. (Springer, 2007), Vol. **15**.
26. B. W. Plansinis, W. R. Donaldson, and G. P. Agrawal, "What is the temporal analog of reflection and refraction of optical beams?" *Phys. Rev. Lett.* **115**, 183901 (2015).
27. N. N. Rosanov, "Transformation of electromagnetic radiation at moving inhomogeneities of a medium," *JETP Lett.* **88**, 501–504 (2008).
28. Z.-L. Deck-Léger and C. Caloz, "Wave scattering by superluminal spacetime slab," arXiv:1611.01366 (2016).
29. B. W. Plansinis, W. R. Donaldson, and G. P. Agrawal, "Spectral splitting of optical pulses inside a dispersive medium at a temporal boundary," *IEEE J. Quantum Electron.* **52**, 6100708 (2016).
30. B. W. Plansinis, W. R. Donaldson, and G. P. Agrawal, "Temporal waveguides for optical pulses," *J. Opt. Soc. Am. B* **33**, 1112–1119 (2016).
31. J. Zhou, G. Zheng, and J. Wu, "Comprehensive study on the concept of temporal optical waveguides," *Phys. Rev. A* **93**, 063847 (2016).
32. D. V. Skryabin and A. V. Yulin, "Theory of generation of new frequencies by mixing of solitons and dispersive waves in optical fibers," *Phys. Rev. E* **72**, 016619 (2005).
33. K. E. Webb, M. Erkintalo, Y. Xu, N. G. R. Broderick, J. M. Dudley, G. Genty, and S. G. Murdoch, "Nonlinear optics of fibre event horizons," *Nat. Commun.* **5**, 4969 (2014).